Influence of Microstructure and Stress on Short Intergranular Stress Corrosion Crack Growth in Austenitic Stainless Steel Type 304

S. Rahimi [1, a], T.J. Marrow [1, b]

[1] School of Materials, The University of Manchester, Grosvenor Street, Manchester, M1 7HS, UK

[a] Salahoddin.Rahimi@postgrad.manchester.ac.uk, [b] james.marrow@manchester.ac.uk

Keywords: Intergranular stress corrosion cracking (IGSCC), grain boundary engineering (GBE), grain boundary character distribution (GBCD)

Abstract

Intergranular stress corrosion cracking (IGSCC) causes failures in austenitic stainless steels when the appropriate electrochemical, metallurgical and mechanical conditions exist. In this study, the effects of time, applied stress, residual stress and microstructure on population of short crack nuclei has been investigated in sensitised type 304 austenitic stainless steel, tested under static load in an acidified potassium tetrathionate (K2S4O6) environment. Statistical analysis, using the Gumbel distribution method, enables analysis of the growth rate of short crack nuclei. This methodology is being developed, in order to quantitatively evaluate the influence of grain boundary engineering and surface finishing on crack nucleation.

Introduction

Austenitic stainless steels due to their superior corrosion resistance, excellent mechanical properties and good weldability are consistently used in oil production, power generation industries and everyday applications [1]. Stress corrosion cracking (SCC) is a phenomenon in which the crack propagates in a susceptible material due to the combined effect of tensile stress and corrosive environment [2, 3]. The susceptibility of austenitic stainless to intergranular corrosion (IG) and intergranular stress corrosion cracking (IGSCC) is increased with sensitisation of particular grain boundaries. Sensitisation in austenitic stainless steels is due to precipitation of chromium rich carbide ($M_{23}C_6$) in the grain boundaries after heat treatment (such as post-weld stress relief). This process causes chromium depletion zones adjacent to grain boundaries [4, 5], which decreases corrosion resistance locally to a degree that influenced by the structure of grain boundaries [6, 7].

Chemical properties and the physical structure of grain boundaries determine the resistance of material to intergranular degradation such as stress corrosion cracking, sensitisation and creep [8]. The structure of grain boundaries has been described by the coincidence site lattice (CSL) model which is related to the crystallographic orientation of adjacent grains [9]. The CSL model is commonly used to classify the grain boundaries into low $\sum$ CSL boundaries ($\leq\Sigma 29$) and random boundaries [8, 9]. Giving this proposition, grain boundary engineering has been able to improve the resistance to intergranular degradation by maximising the fraction of low $\sum$ grain boundaries through thermo-mechanical processes [10, 11].

During the last two decades several predictive models have been introduced to estimate the probability of crack arrest in a microstructure with certain grain boundary network characteristics. These binary models consider a grain boundary to be either resistant or susceptible to SCC, and determine the probability of crack arrest regarding the grain boundary character distribution and network connectivity via the distribution of triple junction [10-12]. In none of these proposed models have the effect of applied stress magnitude and exposure time in aggressive media been taken into account.

Three dimensional in-situ observation of IGSCC in type 302 austenitic stainless steel has revealed crack bridging behavior [13, 14]. Bridging happens due to the superior corrosion resistance of non-sensitised grain boundaries, which are then left behind the propagating crack front in the 3D geometry. Therefore a grain boundary engineered microstructure with a high proportion of resistant boundaries is expected to create more ductile ligaments (bridges) during crack propagation. Models have been developed to estimate the shielding effect of these bridges on stress intensity factor in crack tip, and also the crack growth rate dependency on the grain boundary characteristics [15-17]. The incubation time for crack initiation has found to be longer for thermo-mechanically treated stainless steel [17]. This has been investigated in-situ using digital image correlation (DIC) to observe crack initiation and crack interaction with various microstructural features

Such local observations are useful for the study of mechanisms. However, lifetime prediction relies on statistical data for the largest likely crack that can develop. In this study the relationship between crack growth and exposure time duration and applied stress magnitude has been investigated.

Experimental Details

Material and Heat Treatment:

A type 304 stainless steel with initial dimensions of 1m×1m×13mm (L×W×T) was used for this survey. The material was received in the mill annealed condition and the chemical composition supplied by the manufacturer is given in Table 1. Sample blanks of 240×30×13mm (L×W×T) were cut from the main plate with the length along rolling direction. These blanks were then solution annealed at 1050°C for 2 hours in air atmosphere and cooled down to the room temperature in air. Subsequently, the blanks were sensitised at 650°C for 20 hours in air atmosphere. These sensitised solution annealed blanks were then machined parallel to the rolling plane to the final dimensions of 240×30×7mm (L×W×T), by trimming 1mm material from one side and 5mm from other side to obtain 7mm thick strips.

Metallographic study of material across the thickness was carried out for both as received and solution annealed conditions. This was performed by electro-etching the surface in 10% Oxalic acid and 13V for less than a minute. The surfaces were then investigated using an Olympus-BH2 optical microscope (OM) which was interfaced with a Leica DC200 frame grabber and equipped with an Olympus MS-Plane lens.

Table 1: Nominal composition of stainless steel 304, used in this study supplied by manufacture (wt.%).

Data	*Fe*	*Cr*	*Ni*	*C*	*Mn*	*P*	*S*	*Si*	*N*
Supplier	Bal.	18.15	8.60	0.055	1.38	0.032	0.005	0.45	0.38

Surface Optimisation and Loading

The as-machined strips were subjected to an electro-polishing process to remove the residual stress introduced by the machining stage. The electrolyte solution was a mixture of acetic acid (92 % wt) and perchloric acid (8 % wt) and the cathode was stainless steel type 304 sheet with approximate dimensions of 19cm×8cm×0.5mm (L×W×T). The specimens immersed in the electrolyte solution at 45 V.

To optimise the electro-polishing time duration, XRD measurements using a Proto i-XRD portable stress diffractometer were performed in eight points at intervals of 7 mm to determine the longitudinal ($\varphi = 0^o$) and transverse ($\varphi = 90^o$) stresses at position along the middle fibre within the 80 mm gauge length of selected strips (Figure 1). For each point ten measurements were performed in both directions ($\varphi = 0^o$ and $\varphi = 90^o$) with an exposure time for each measurement of one second.

This was carried out on the as-machined surface and after 10, 20, 40, 60 minutes electro-polishing. Ultimately, 60 minutes electro-polishing was chosen for all strips to attain stress free surfaces for the stress corrosion tests.

In order to produce a static tensile elastic stress to perform stress corrosion cracking experiments, the double bend beam form was chosen from the ASTM standard [18]. The double bend beam (DBB) sample is composed of two strips with the same microstructure and dimensions, and a spacer. The strips were bent against each other over the spacer, with the ends of the strips held together by a bolt in each corner of the strips. The DBB specimen is self contained and is schematically shown in Figure 1. Spacer thicknesses of 1.5mm, 3mm and 4mm were used to obtain nominal stress magnitudes of 100, 200 and 260 MPa respectively. XRD measurements on electro-polished and loaded samples were obtained to evaluate the magnitudes of applied stresses in comparison with calculated stresses. Measurements were also performed on samples which had been loaded, and then unloaded.

Exposure and Statistical Analyses

The loaded specimens were exposed in approximately 250ml solution of 0.1M potassium tetrathionate ($K_2S_4O_6$ in deionised water) with a pH of 2 for times of 72, 144, 288 and 432 hours. The pH was adjusted by adding dilute sulphuric acid. After exposure the DBB specimens were unloaded and the separate halves of the sample were pulled for 5% (measured using an extensometer with 20 mm gauge length) in order to open the cracks sufficiently to make them visible by optical microscopy. The middle portion of the pulled specimens between the spacer contact point lines (i.e. the exposed portion) was cut transversely to remove it from the specimen. It was then cut longitudinally into three pieces using a 0.5mm thick diamond saw. The pieces were then mounted in cold casting resin (Kleer SET Type FF / Metprep). A perpendicular section was also prepared along the spacer contact point lines. All samples were ground and polished to a mirror like finish. The 4 longitudinal slices from each sample, each 80 mm in length, were examined in successive 2mm wide areas in order to record the deepest crack in each area by optical microscopy.

The recorded crack length population was then assessed using extreme value statistics [19]. In this approach the collected data is tested using a distribution type based on observation of the longer cracks in the population. This extreme value analysis allows comparison of crack length distributions, without measurement of every crack in each sample. In this study, a doubly exponential, first type maximum value distribution had been used. This assessment obtains the longest likely crack in the specimen, which derives from a parent distribution with an exponentially decreasing tail function [19]. Eq 1 was used to calculate the reduced parameter (Y), which can be plotted as a function of measured crack size.

$$Y = -\ln(-\ln(P_i)) \qquad \textbf{(1)}$$

Where $P = \dfrac{i}{n+1}$ is the empirical cumulative probability of the ith data point, n is the total number of crack measurements and i is the position in an ascending list of crack length [20].

Results

The material composition is in the range of the austenitic stainless steel type 304 defined by the standard [21]. Metallographic investigation shows that there is significant heterogeneity in the microstructure across the thickness of the plate in as-received conditions in terms of grain size and the concentration of δ-ferrite (Figure 2). The grain size is coarse close to the edges and tends to decrease towards the middle of the plate. Interestingly, the minimum grain size is not exactly in the centre of the plate. The presence of a significant amount of ferrite bands in the middle is also detected. After 2 hours solution annealing at 1050°C the grain size variation remains similar but due

to grain growth the overall grain size has been increased. The fraction of δ-ferrite in solution annealed condition also has a similar trend to the as-received material, but the total content is significantly reduced. The percentage of δ-ferrite in as received microstructure is negligible close to the edges and is increases gradually up to ~10% in the middle. After solution annealing the δ-ferrite percentage reached a maximum of ~ 4% in the middle of the sample.

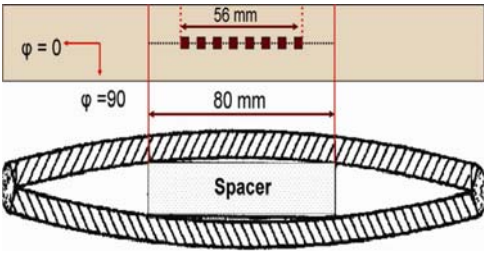

Figure 1: Double bent beam (DBB) specimen. The theoretically uniform stress region is enveloped between two red lines and the top view shows the schematic positions of the analysed points by XRD. The sample bend is exaggerated.

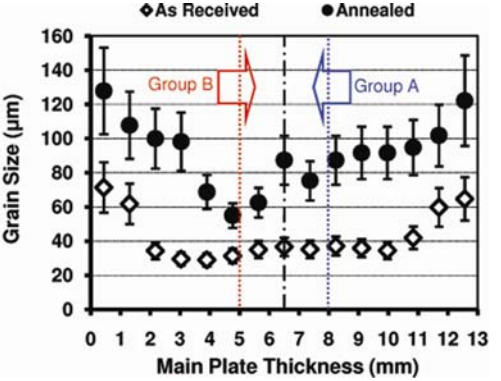

Figure 2: Grain size variation across the main plate (13mm thick). The surface grain sizes of both groups of specimens have been indicated by arrows.

The IGSCC specimens had been trimmed down from the initial thickness of 13 mm of the main plate into the final thickness of 7 mm by removing 1 mm from one side and 5 mm from other side through machining process. Depending on the surface from which the 5 mm was removed, the samples fell into either of two groups (A and B). The position of the surface tested in the SCC experiments for each group is identified in Figure 2. Optical micrographs adjacent to the exposed surface are shown in Figure 3, for samples examined after SCC testing. A significant variation in grain size is obtained between the two groups.

The electro-polishing duration time and amount of material that should have removed to eliminate the residual stresses introduced by machining were found by measuring the surface strain by XRD in as machined condition and after removing various amounts of material. Measurements in two directions of longitudinal ($\varphi = 0^o$) and transverse ($\varphi = 90^o$) are shown in Figure 4a. One hour electro-polishing gives an effectively stress-free surface and was chosen as the optimum time to reach the surface free residual stress for all strips. Typical stress measurements along the middle fibre in the longitudinal ($\varphi = 0$) direction for three expected magnitude of stresses of 100, 200 and 260 MPa used for the IGSCC tests are given in Figure 4b.

The results of the statistical evaluation of crack lengths in the constant stresses and various exposure times are shown in Figure 5a, 5b, and 5c for nominal stresses of 100, 200 and 260 MPa respectively. In these graphs, the solid symbols are for Group A and open symbols are for Group B. The average grain size at the surface was 85μm for group A and 55μm for group B. There is a general trend for greater crack size in the group A samples, and both groups tend to show longer cracks with higher stress and longer exposure time. These can be more clearly seen by considering the expected crack length at constant Y in Figures 5. Figures 6(a, b) show the crack lengths in $Y = 1$ and $Y = 3$ respectively. Based on Eq (1), in a particular constant Y the empirical cumulative probability (P_i) is equal to a certain value corresponding to the ith data point, which in this case for Y equal to 2 and 3 the P_i are 0.88 and 0.95 respectively. This means the probabilities of finding a crack exceeding this size in the inspected area are 12% and 5% respectively. The values are obtained as the best fit to the Gumbel distribution, with a confidence interval of 95%.

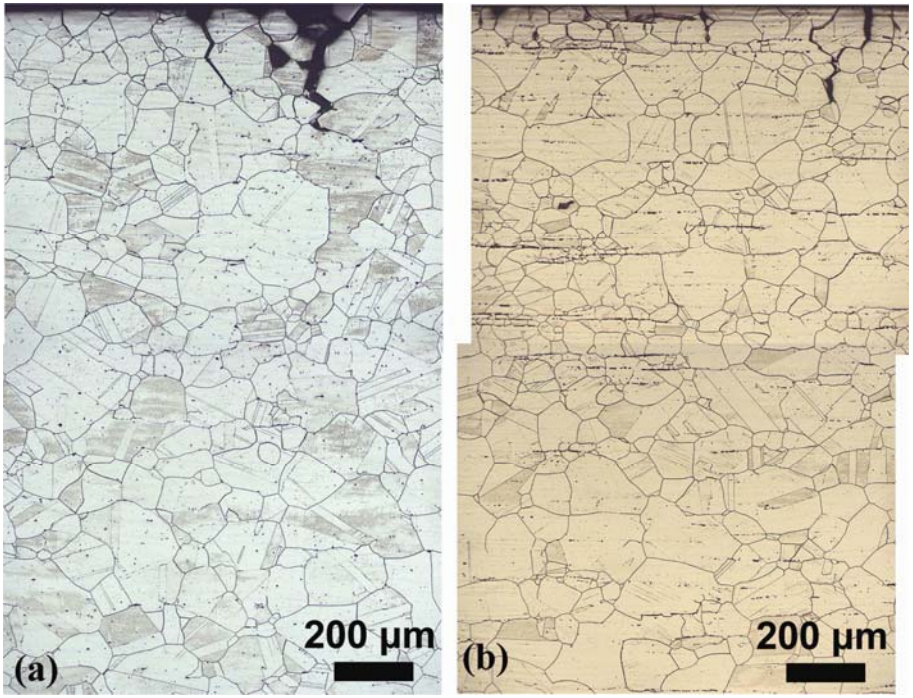

Figure 1: Optical micrograph of the microstructure across the thickness from exposed surface toward the middle (a) Group A and (b) Group B.

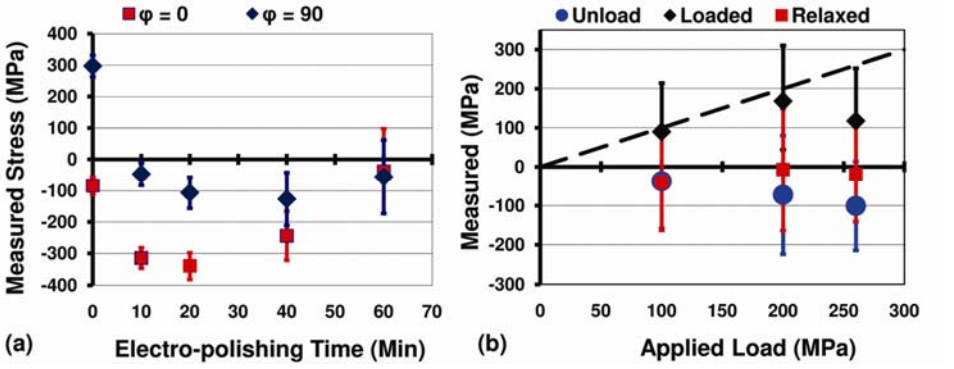

Figure 2: Stress measurement by XRD, (a) Effect of electro-polishing time duration on residual stress magnitude, (b) Measured longitudinal stress magnitude in three conditions of unload (after 1 hour electro-polishing), loaded (in comparison with calculated stress) and relaxed by opening the DBB.

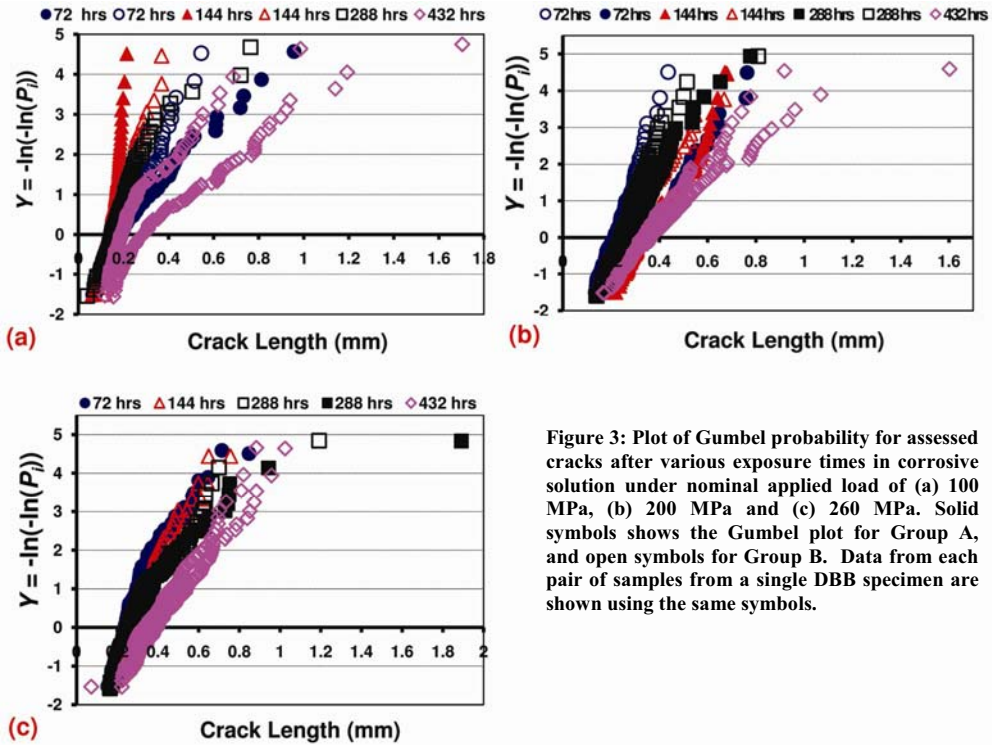

Figure 3: Plot of Gumbel probability for assessed cracks after various exposure times in corrosive solution under nominal applied load of (a) 100 MPa, (b) 200 MPa and (c) 260 MPa. Solid symbols shows the Gumbel plot for Group A, and open symbols for Group B. Data from each pair of samples from a single DBB specimen are shown using the same symbols.

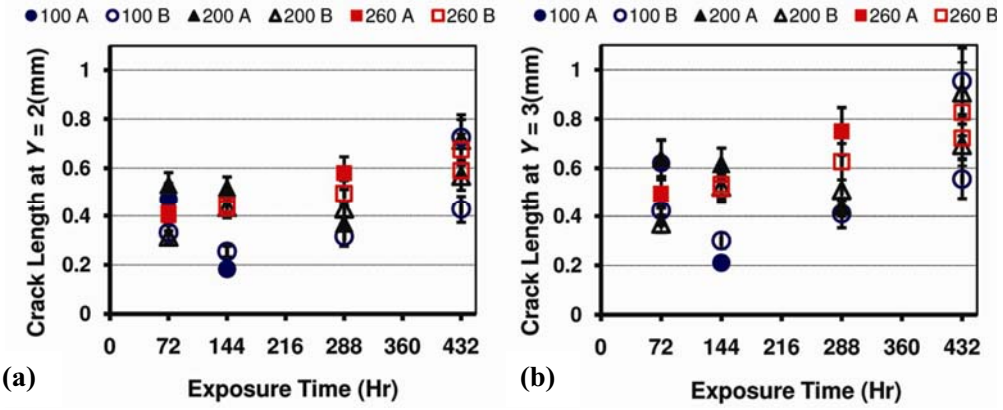

Figure 4: The expected maximum crack length, at (a) *Y*=2 and (b) *Y*=3.

Discussion

In all cases the material removed after one hour electro-polishing was between 100µm to 150µm. Although the XRD measurements have errors due to the large grain sizes of the solution annealed material and surface unevenness after electro-polishing, it can be concluded from Figure 4a that 1 hour is sufficient to ensure that the surface was free from significant residual stress from machining. The applied stresses at 100 and 200 MPa are shown, by the XRD measurements, to be in good

agreement with the nominal applied stress. The yield strength (0.2% proof stress) for this plate of type 304 stainless steel in a solution annealed condition (1050 °C for 30 minutes) has been previously measured to be 210 MPa [22]. Hence it can be expected that the surface of those samples loaded to 260MPa was strained above yield stress. This is consistent with Figure 4b, which shows that the loading to 100 and 200 MPa was essentially elastic, whereas loading to a nominal stress of 260 MPa caused specimen yield with no proportional increase in the measured stress with applied stress.

The statistical data for the crack populations show that crack length tends to increase with test duration, and that longer cracks tend to be observed in the coarser microstructure for group A. The data are, however, insufficient to form any conclusions on relative crack growth rates, despite the large number of cracks measured. A decrease in the rate of development of short intergranular stress corrosion crack nuclei with decreasing grain size is predicted by the crack bridging models [14, 15].

The effect of stress is less clear in Figure 6. The crack bridging models for IGSCC predict faster growth of short crack nuclei with higher stress. However, although there is a tendency for shorter cracks at 100 MPa, some samples gave much longer crack lengths that the higher stress tests (e.g. Figure 6b). Similar crack lengths are obtained for the tests at 200 and 260 MPa – this is understandable on the basis that both experience very similar stress due to yielding of the higher stressed sample. The data in Figure 6 suggest that there is an underlying effect of stress on crack development, but it is less significant than the scatter in the data.

One cause of this variability may be microstructural heterogeneity. Nominally identical samples could present quite significant differences in surface microstructure for small differences in the position of the surface relative to the original plate surface. This is evident from Figure 3, in which significant changes in grain size exist over quite short distances. The crack lengths developed in these tests are of the order of 5-7 grains; hence the population of cracks developed within coarse or fine grained regions close to the sample surface could show significant variability.

Short crack behaviour is strongly influenced by the local microstructure. Prediction of crack populations therefore requires an understanding of the heterogeneity of microstructure as well as the interaction between an individual crack and microstructure. This can be achieved using in-situ observations of short crack behaviour (e.g. [17, 23]), in combination with the statistical approach used in this paper.

Conclusion

Analysis of intergranular stress corrosion crack populations in sensitised type 304 stainless steel, tested under static load, using extreme value statistics (Gumbel analysis), shows an increase in the expected crack length with increasing time and grain size. The crack lengths tend to increase with stress, but the effect is less significant than the variability in the crack populations. This variability may be due to heterogeneity in the microstructure.

References

1. Marshal, P., Austenitic Stainless Steels, Microstructure and Mechanical Properties. 1984: Elsevier applied Science.
2. Hanninen, H.E., Stress Corrosion Cracking. Comprehensive Structural Integrity, 2003. 6: p. 1-29.
3. Newman, R.C., Stress-Corrosion Cracking Mechanisms, in Corrosion Mechanisms in Theory and Practice, P. Marcus, Editor. 2002, MARCEL DEKKER. p. 399-450.
4. Ortner, S.R., A STEM study of the effect of precipitation on grain boundary chemistry in AISI 304 Steel. Acta. Metall. Mater, 1991. 39(3): p. 341-350.

5. V. Kain, R.C.P., and P.K. De, Testing Sensitization and Predicting Susceptibility to Intergranular Corrosion and Intergranular Stress Corrosion Cracking in Austenitic Stainless Steels. 2002. 58(1): p. 15-37.

6. Bruemmer, S.M.W., G. S, Microstructural and microchemical mechanisms controlling intergranular stress corrosion cracking in light-water-reactor systems. Journal of Nuclear Materials, 1994. 216: p. 348-363.

7. Zhou, Y., Aust, K. T., Erb, U. & Palumbo, G, Effects of grain boundary structure on carbide precipitation in 304l stainless steel. Scripta Materialia, 2001. 45(1): p. 49-54.

8. Davies, P., Randle, V., Literature, Review: Grain boundary engineering and the role of the interfacial plane. Materials Science and Technology, 2001. 17(June): p. 615 - 626.

9. Randle, V., The role of the coincidence site lattice in grain boundary engineering. 1996, London: Institute of Materials.

10. Palumbo, G., King, P. J., Aust, K. T., Erb, U. & Lichtenberger, P. C., Grain boundary design and control for intergranular stresss-corrosion resistance. Scripta Metallurgica et Materialia, 1991. 25: p. 1775-1780.

11. Lehockey, E.M., Brennenstuhl, A. M. & Thompson, I, On the relationship between grain boundary connectivity, coincident site lattice boundaries, and intergranular stress corrosion cracking. Corrosion Science, 2004. 46(10): p. 2383-2404.

12. Gertsman, V.Y., Janecek, M., Tangri, K., Acta Materialia, 1996. 44: p. 2869.

13. Babout, L., Marrow, T. J., Engelberg, D. & Withers, P. J., X-ray microtomographic observation of intergranular stress corrosion cracking in sensitised austenitic stainless steel. Materials Science & Technology, 2006. 22(9): p. 1068-1075.

14. Marrow, T.J., Babout, L., Jivkov, A., Wood, P., Engelberg, D., Stevens, N., Withers, P. J. & Newman, R. C., Three dimensional observations and modelling of intergranular stress corrosion cracking in austenitic stainless steel. Journal of Nuclear Materials, 2006. 352: p. 62-74.

15. Jivkov, A.P., Stevens, N. P. C. & Marrow, Z. J., A three-dimensional computational model for intergranular cracking. Computational Materials Science, 2006. 38: p. 442-453.

16. Jivkov, A.P., Stevens, N. P. C. & Marrow, T. J., Meso-scale mechanical model for intergranular stress corrosion cracking and implications for microstructure engineering. Journal of Pressure Vessels Technology - Transactions of the ASME, 2007. In Press.

17. Rahimi, S., Duff, J. A., Engelberg, D. L., Marrow, T. J., In-situ Observation of Intergranular Crack Nucleation in Grain Boundary Controlled Austenitic Stainless Steel. Submitted to the Journal of Microscopy, 2008.

18. ASTM G39-99, Standard Practice for Preparation and Use of Bent-Beam Stress-Corrosion Test Specimens, 2000.

19. Kowaka, M., Introduction to life prediction of industrial plant materials: application of the extreme value statistical method for corrosion analysis. 1994, New York: Allerton Press.

20. Beretta, S., Anderson, C., Murakami, Y., Extreme value models for the assessment of steels containing multiple types of inclusion. Acta Materialia, 2006. 54: p. 2277 - 2289.

21. ASTM A240M, Standard Specification For Chromium and Chromium-Nickel Stainless Steel Plate, Sheet and Strip for Pressure Vessels and for General Applications. 2002.

22. Engelberg, D.L., Grain Boundary Engineering for Intergranular Stress Corrosion Resistance in Austenitic Stainless Steel. 2005, The University of Manchester & UMIST: Manchester.

23. Duff, J.A., Marrow, T. J. In-situ observation of intergranular stress corrosion cracking. in PVP2008 - Pressure Vessels and Piping Conference. Chicago, Illinois. 2008.